Fusion Engineering and Design 122 (2017) 313–321

Contents lists available at ScienceDirect

Fusion Engineering and Design

journal homepage: www.elsevier.com/locate/fusengdes

The DTT device: Power and particle exhaust

R. Zagórski[a,*], V. Pericoli Ridolfini[a,b], F. Subba[c], F. Crisanti[b], G. Giruzzi[d], H. Reimerdes[e], G. Rubino[b]

[a] Institute of Plasma Physics and Laser Microfusion, 01-497 Warsaw, Poland
[b] ENEA-Frascati, Via E. Fermi 45, 00044 Frascati Italy
[c] Politecnico di Torino, Italy
[d] CEA, DRFC/CEA/Cadarache, 13108 St. Paul-lez-Durance, France
[e] Ecole Polytechnique Federale de Lausanne, Centre de Recherches en Physique des Plasmas, Suisse, 1015, Lausanne, Switzerland

HIGHLIGHTS

- Scenarios at full power of the DTT device with the standard single null and X divertor configurations have been analysed for the aspect of divertor heat loads mitigation.
- It has been shown that with Ne and Ar seeding it is possible to achieve H-mode plasma operation with acceptable level of the power to the tungsten target plates.
- TECXY simulations show that in term of global parameters little difference exists between the two divertor configurations for low working densities.
- The situation shows different at higher density where the X divertor seems indeed to favour detached operations and strongly radiating regimes.

ARTICLE INFO

Article history:
Received 29 July 2016
Received in revised form 24 May 2017
Accepted 24 May 2017
Available online 7 June 2017

Keywords:
DTT project
Tokamak
Power exhaust
Impurity radiation
Plasma modelling

ABSTRACT

The possible scenarios at full power of the DTT (Divertor Test Tokamak) device with the standard single null (SN) and X divertor (XD) configurations have been analysed for the aspect of safely handling the power to be exhausted on the divertor targets. In this conceptual design phase the computational tools have been chosen mainly on the basis of their simplicity and rapidity. The code COREDIV was used for a preliminary self-consistent description of the coupled edge-core system. Subsequently, a more punctual analysis has been carried out on the SOL with the TECXY code. COREDIV results show that operations without impurity seeding may be problematic in all scenarios, and especially at the higher densities where tungsten is virtually absent in the core and the core radiation very low.

The main outcome of this study is that in term of global parameters little difference exists between the two configurations for low working densities. The reason is identified in the fact that the topology modifications occur in region where the dissipative processes, radiation inelastic collisions etc., are rather negligible to be enhanced at significant level.

The situation shows different at higher density where the XD seems indeed to favour detached operations and strongly radiating regimes. This trend is reinforced by lowering the power entering the SOL and by faster cross-field diffusion. These very important regimes seem to be reachable by the advanced configurations of DTT, for some appropriate choice of the working parameters.

1. Power and particle exhaust in DTT

DTT facility has been proposed to tackle the integrated bulk-edge power exhaust problem and to find out a reliable and robust solution for DEMO [1,2]; the main parameters of the facility are summarized in the Table 1, and the "rationale" for the choice of these parameters can be found in [3]. Within this reference are reported all the mains physics parameters characterizing the power exhaust problem and how they must/can scaled down from DEMO to a smaller facility. Here it is worth to mention that highest diverter plates power flux, compatible with the present technology and materials is of the order of 10÷20 MW/m^2, where the highest value can be sustained only transiently and the lowest is the highest safe one for the stationary phase; a physics parameter often used

* Corresponding author.
E-mail address: Roman.Zagorski@ipplm.pl (R. Zagórski).

http://dx.doi.org/10.1016/j.fusengdes.2017.05.114
0920-3796/

Table 1
DTT parameters.

R (m)	2.15
a(m)	0.70
I_p (MA)	6.0
B_T (T)	6.0
V_p (m^3)	33
($10^{20} m^{-3}$)	1.72
$/n_G$	0.45
P_{Tot} (MW)	45
P_{SEP}/R(MW/m)	15
τ_E (s) (H_{98} = 1)	0.47
(KeV)	6.2
β_N	1.5
Pulse Length (s)	100

to characterize the power exhaust problem is P_{SEP}/R (where P_{SEP} is power flowing from the last magnetic surface) that for a safe DEMO operation must be lower than $15 \div 10\,MW/m^2$. We started the exploration of the divertor operating conditions with modelling tools able to produce in this phase of the project meaningful results in a reasonable lapse of time. Clearly this implies using codes simpler than the most sophisticated ones presently available in the scientific community. Nevertheless the produced overview should outline the peculiarities, if any, of the DTT operating scenarios and provide sound inputs for a subsequent more complex analysis. Furthermore the plasma and device details necessary for a rigorous simulation are still not completely defined. Having in mind this necessity to work out the most important features of the proposed facility, without the necessity to analyse the details (that eventually will the targets of the future experiments), we have followed the following procedure. Since the "power exhaust" problem is a fully integrated bulk-edge problem, a "simple" code (COREDIV [4]) coupling the plasma bulk and the plasma edge. This analysis allows having a set of meaningful set of input parameters for a simplified 2D edge code (TECXY [5]) that has been used to explore in a fast way the largest of possible experimental scenarios. Eventually the results of TECXY have been "verified" by using the more complete EDGE2D-EIRENE [6,7] reference code for a subset of possible scenarios.

The first step has been to analyse the general plasma performance by means of the system code METIS [8] (a relatively simple energy transport code) in order to check the consistency of the results with the assumption for the boundary conditions of the Scrape-Off Layer (SOL). The subsequent step has been to use this information for validating and detailing the scenario with the COREDIV code [4], which couples the 1D plasma transport in the core and 2D multi-fluid transport in the SOL. In this code the coupling SOL-core is given by imposing the continuity of energy and particle fluxes, densities and temperatures at the separatrix, and by using the computed fluxes from the core as boundary conditions for the SOL. In turn, the temperatures and densities calculated in the SOL (averaged values along the separatrix from stagnation to X point) are used as boundary conditions for the core module. In the core, the 1D radial transport equations for bulk ions, for each ionization state of impurity ions and for the electron and ion temperature are solved; since DTT facility will not have strong injection of external momentum, for this preliminary analysis no rotation has been considered. All ions have the same temperature. Line radiation and bremsstrahlung determine the energy losses, non-coronal effects are included. Neoclassical transport is considered in the bulk, with a contribution from anomalous transport that is scaled to reproduce the prescribed energy confinement, namely the ITER-98y2 ELMy H-mode scaling [9] in the present calculations. The plasma density profile is given by the solution of the radial diffusion equation. The source intensity is determined by the internal iteration procedure in such a way that the average electron density obtained from neutrality condition equals that of the scenario considered. The impurity transport is described by the standard neoclassical (collisionality dependent) and anomalous transport. The anomalous impurity transport includes only a diffusive term, since the anomalous pinch velocity is set to zero.

The 2D multi-fluid model in the SOL and divertor region is based on Braginskij-like equations [10] for the background plasma and rate equations for the ionization state of each impurity species. These latter can be both added and intrinsic, i.e. sputtered from the target plates. The various ion species in their different charge states are treated as separate fluids but all at the same temperature T_i, distinct from that of the electron fluid, T_e. The continuity, parallel momentum and energy equations are solved. For the neutrals an analytical description is assumed with an assigned recycling coefficient. The transport along field lines is assumed to be classical and transport coefficients follow from the 21-moment Grad approximation. The parallel velocities and the gradients of densities and temperatures are assumed to be zero at the midplane (stagnation point). The radial transport is anomalous with prescribed radial transport coefficients ($D_\perp = 0.5\,m^2/s$, $\chi_{e\perp} = 1.0\,m^2/s$, $\chi_{i\perp} = 0.5\,m^2/s$), that reflects in a heat flux e-folding length of the order of 1 cm. This is not e-folding length predicted by the Eich scaling [11] for the reference scenario DTT, that it is of the order of a few millimetres; however, since the SOL is modelled by a simple slab geometry (poloidal and radial directions) that neglects both the real divertor geometry and a possible flux expansion at the plate, only the total divertor load is here considered, not its distribution along the target. In any case the validity of this assumption is supported by the overall negligible effect of varying the edge transport parameters for some selected cases. The standard sheath boundary conditions are imposed at the plates and the plasma is assumed to be in the attached mode. Of course this will not be the real experimental situation mainly at high density, where the plasma will be a "semi-detached" phase; however, since the main scope of this analysis is to find out whether and under which conditions, the plasma can approach a detached "situation", this hypothesis is quite robust.

The main limitations of this modelling can be identified in the lack of pedestals, in the missing drifts and in the absence of the impurity anomalous pinch. A temperature pedestal may lead to a broadening of the radiation zone inside the separatrix. The effect of the drifts would be concentrated in the SOL and in the boundary region close to the separatrix, where they might affect transport significantly, due to their interrelation with the radial electric field and its shear. Nevertheless the absence of drifts in COREDIV does not lead to a significant loss of generality of our results since their influence on the core contamination and on the global energy balance of the relatively high density plasmas is expected to be rather small. Moreover the high magnetic field in DTT (<6.5 T) would tend to suppress the drifts effects.

Both in the core and in the SOL therefore the impurity fluxes and the associated radiation losses are calculated fully self-consistently, as well as the energy losses due to interactions with hydrogenic atoms (line radiation, ionization and charge exchange).

The target material is assumed to be tungsten. The additional impurities considered in these first simulations to mitigate the thermal loads are N or Ar, puffed from the divertor region.

Validation of the COREDIV code comes from the successful simulations of N and Ne seeded JET discharges [12,13] JET in ITER like wall configuration [14] and Asdex Upgrade (AUG) with full tungsten wall [15].

Three different volume averaged densities have been considered: the reference one, $\langle n_e \rangle_{ref}$, one lower $\langle n_e \rangle_{low}$, and one higher, $\langle n_e \rangle_{high}$, respectively = 1.8, 1.0, $2.5 \times 10^{20}\,m^{-3}$ (corresponding to n/n_G 0.5, 0.3, 0.7; where n_G is the Greenwald density limit) with a correspondent density at the separatrix of 0.74, 0.49 $1.0 \times 10^{20}\,m^{-3}$. Constant have been kept the macroscopic parameters, plasma cur-

Table 2
COREDIV results for $\langle n_e \rangle_{ref} = 1.8 \times 10^{20}$ m^{-3}; $n_{e,sep} = 7.4 \times 10^{19}$ m^{-3}.

	W only	W + N – I	W + N II	W + Ar
$\Gamma_{puff,Z}$ (10^{20} s^{-1})	/	5	20	1
$Z_{eff,0}$	1.02	1.29	1.51	1.45
T_{e0} (keV)	12.8	13.8	14.6	14.6
n_W (%)	5.2×10^{-4}	7.5×10^{-3}	1.0×10^{-2}	1.0×10^{-2}
$n_{Ar,N}$ (%)	0	8.3×10^{-2}	0.41	3.35×10^{-2}
$f_{rad,tot}$ (%)	12.3	44.7	62.1	61.7
P_{SOL} (MW)	36.7	24.7	19.4	18.5
P_{plate} (MW)	32.0	19.6	12.7	12.8
$f_{loss,SOL}$ (%)	12.9	20.8	34.5	30.6
$T_{e,sep}$(eV)	210	178	161	157
$n_{e,plate}$ (10^{19} m^{-3})	39.7	58.4	67.8	64
T_{plate} (eV)	29.6	14.5	6.8	7.2

Table 3
COREDIV results for $\langle n_e \rangle_{low} = 1.0 \times 10^{20}$ m^{-3}; $n_{e,sep} = 4.9 \times 10^{19}$ m^{-3}.

	W only	W + N I	W + N II	W + Ar I	W + Ar II
$\Gamma_{puff,Z}$ (10^{20} s^{-1})	/	5	10	1	2
$\Gamma_{p,SOL}$ (10^{21} s^{-1})	1.82	1.59	1.43	1.28	1.18
$Z_{eff,0}$	1.59	2.17	2.56	2.89	3.46
T_{e0} (keV)	19.2	19.91	20.65	21.6	22.5
n_W (%)	0.017	0.032	0.04	0.047	0.049
$n_{Ar,N}$ (%)	0	0.15	0.356	0.072	0.24
$f_{rad,tot}$ (%)	22.5	39.7	52.4	65.3	74.2
P_{SOL} (MW)	32.4	26.1	21.5	16.4	13.9
P_{plate} (MW)	28.7	22.2	17.3	12.13	8.6
$f_{loss,SOL}$ (%)	11.7	15.1	19.7	26.2	38.2
$T_{e,sep}$(eV)	218	194	176	152	140
$n_{e,plate}$ (10^{19} m^{-3})	16.6	22.3	28.8	33.5	41.3
T_{plate} (eV)	57.8	33.2	21.9	13.8	8

Table 4
COREDIV results for $\langle n_e \rangle_{high} = 2.5 \times 10^{20}$ m^{-3}; $n_{e,sep} = 1. \times 10^{20}$ m^{-3}.

	W only	W + N I	W + N II	W + Ar I
$\Gamma_{puff,Z}$ (10^{20} s^{-1})	/	3	5	3
$\Gamma_{p,SOL}$ (10^{21} s^{-1})	5.1	4.74	4.62	4.1
$Z_{eff,0}$	1	1.05	1.07	1.25
T_{e0} (keV)	11.02	11.3	11.4	12
n_W (%)	0	0.001	0.001	0.002
$n_{Ar,N}$ (%)	0	0.032	0.054	0.056
$f_{rad,tot}$ (%)	18.2	30.8	35.2	55.7
P_{SOL} (MW)	36.8	32.4	30.9	25.3
P_{plate} (MW)	28.5	23.5	21.7	12.9
$f_{loss,SOL}$ (%)	22.5	27.5	29.9	48.8
$T_{e,sep}$(eV)	185	176	173	159
$n_{e,plate}$ (10^{19} m^{-3})	104	109	111	119
T_{plate} (eV)	9.4	6.4	5.7	3.1

rent, magnetic field and auxiliary power, respectively: $I_p = 6.0$ MA; $B_T = 6.0$ T; $P_{aux} = 40$ MW. The outputs are given below in Tables 2–4 .

As compared with the calculations performed for FAST [16] with $P_{aux} = 40$ MW we see that the loads are slightly increased mostly because of the smaller working density. This increment is however balanced by the larger major radius if the specific loads are concerned. A similar reasoning is valid in the no impurity seeding simulations.

A preliminary selection of the acceptable scenarios from the heat load point of view can be made from the following simple arguments on the expected width of the power flow channel in the outboard equator Δ_{eq}. According to the present scaling law [11], $\Delta_{eq} \approx 4$ mm is a reasonable value for DTT if we add the effect of the diffusion into the divertor private region that COREDIV neglects. Assuming a flux expansion by 5 times onto the target, usual for a conventional standard divertor Single Null (SN) configuration, we get at target $\Delta_{target} = 2$ cm, which in turn can rises up to $\Delta_{target} \approx 6$ cm, due to the target tilting, corresponding to a strike angle for the poloidal field $\approx 20^\circ$, value hard to be further lowered. If the maximum safe load is taken as $P_L = 15$ MW/m^2 and the load is equally shared between the two plates, we get the maximum acceptable upstream power, to be shared by the two plates $P_{max} = 2 \times P_L \times \Delta_{target} \times (2\pi R) = 23.7$ MW for a major radius of the device R = 2.1 m (here the factor two accounts for the two inboard and outboard plates).

2. 2D edge simulations with TECXY

The above tables suggest that operations without impurity seeding may be problematic in all scenarios, and especially at the higher densities where tungsten is virtually absent in the core and the core radiation very low. In the reference scenario a small puff rate of either Ar or N will permit operations at $Z_{eff} \leq 1.5$. At low density a higher Z_{eff} (>2.5) should be accepted for a safe operation, whereas at the highest density the Ar or N injection rates so far considered seem still too poor. This preliminary analysis performed with the COREDIV code depicts a rather border-line situation where the radiation is playing a very important role. Consequently, the simplified 2D transport edge code TECXY [5] has been used to perform a parameters scan to analyse whether experimental scenarios, limited to pure D_2 plasma, could approach detached situations under some real divertor magnetic topology. The detailed effect of the seeding with impurities will be the object of future work, when the detailed studies of the experimental scenarios will be performed. On the other hand, more complex codes, as EDGE2D-EIRENE [6,7], SOLPS-EIRENE [17,18], SOLEDGE2D-EIRENE [19] or ECM3 [20] are not particularly suited at this stage due to the very long running times. The main reason for the rapidity of TECXY is the simple analytical treatment of the neutral dynamics instead of the Monte Carlo technique. All the other main physical features are the same as for the other codes. The actual magnetic topology is taken into account whereas the divertor geometry is simplified with target perpendicular to the poloidal field B_{pol}. This indeed has negligible effect within the analytical neutral model, contrarily to the Monte Carlo case, and avoids, on the other hand, to distort the computing mesh close to targets. Preserving the ideal cell form with two sides perpendicular and two parallel to B_{pol} allows solving more accurately the differential equations. The actual fluxes are recovered simply by multiplying the output by $\sin\alpha_t$, being α_t the angle between B_{pol} and the local poloidal target trace.

Validation of TECXY stems also from having successfully described experiments as Tore Supra [21], FTU [22], TEXTOR [23,24] and the recent AC configuration in EAST [25]. Further the results obtained for the DEMO SOL [26] global quantities and target loads satisfactorily compare to those from EDGE2D-EIRENE [26,27] and SOLPS-EIRENE [26,28].

In this phase we consider only the standard and extended divertor configurations, SN and XD respectively. We note that in some past papers analysing advanced divertors, as those referring to the projected tokamak FAST [16,29] this type of configuration has also been labelled QSF, Quasi-Snow Flake. The two mentioned configurations are sketched in Fig. 1 (full poloidal section) and Fig. 2 (zoom on the divertor region). In XD two secondary nulls of B_{pol} external to the main vessel are added on both the inner and outer divertor leg. For this latter this X point is clearly visible in Fig. 1 (right frame). Consequently, the poloidal flux is expanded, as evidenced by comparing the right with the left side of Fig. 2. Because of the still undefined divertor shape a very rough wall boundary is assumed for both configurations, the green line in the mentioned figures. Consequently, only a relative comparison can be done between the two configurations, the absolute values being meaningless at this stage. The target position is assumed to be located just at the end of the flux lines shown in Fig. 2. The corresponding flux expansions

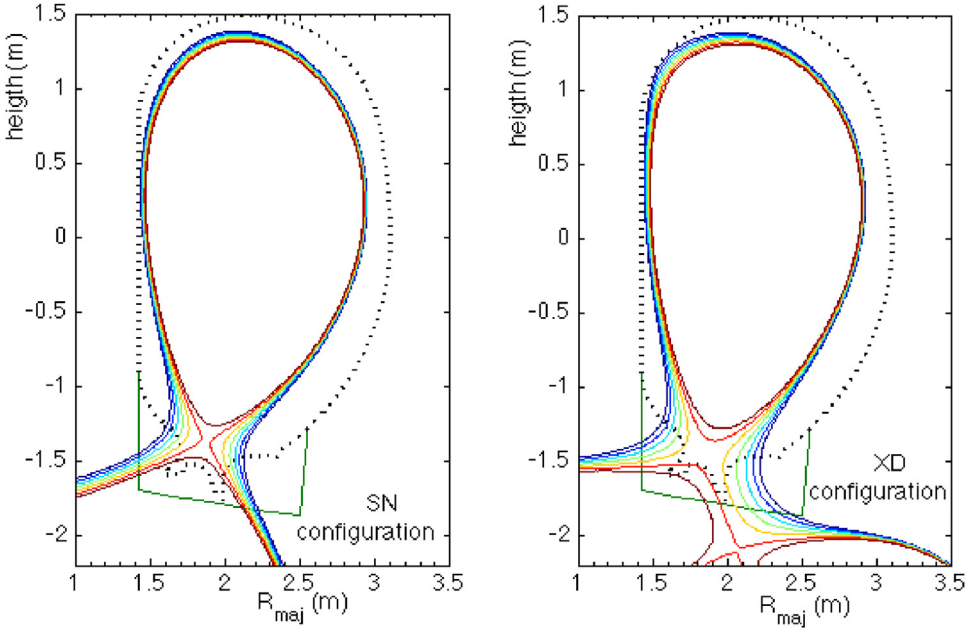

Fig. 1. Computed equilibria of SN (left) and XD (right). The wall shape suitable for SN is shown with a dashed black curve. The shape assumed for all configuration assumed in this paper is show as a green continuous line. (For interpretation of the references to colour in this figure legend, the reader is referred to the web version of this article.)

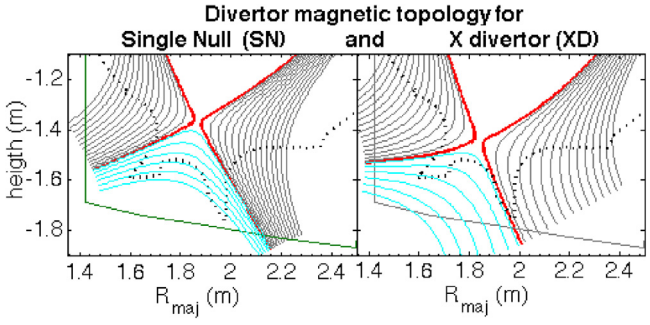

Fig. 2. Details of the divertor region for the computed equilibria of SN (left) and XD (right).

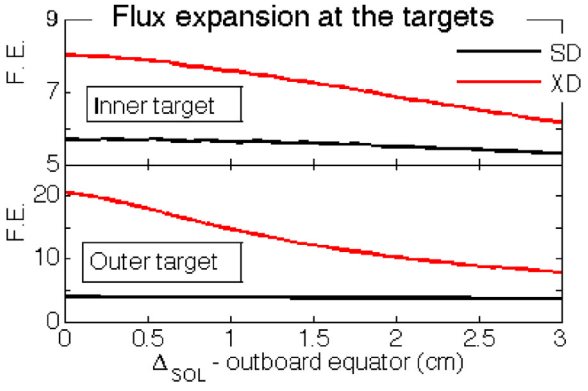

Fig. 3. Flux expansion (F.E.) for SN (black) and XD (red) on both targets versus the outboard equatorial SOL depth. F.E is defined as the ratio of the distance between two adjacent flux lines at the target and at the ouboard equator. (For interpretation of the references to colour in this figure legend, the reader is referred to the web version of this article.)

at the inner and outer target (IT, OT) – ratio between the distance of two adjacent flux surfaces at the target and at the outer equator – are plotted in Fig. 3 versus the outer equatorial distance from the separatrix.

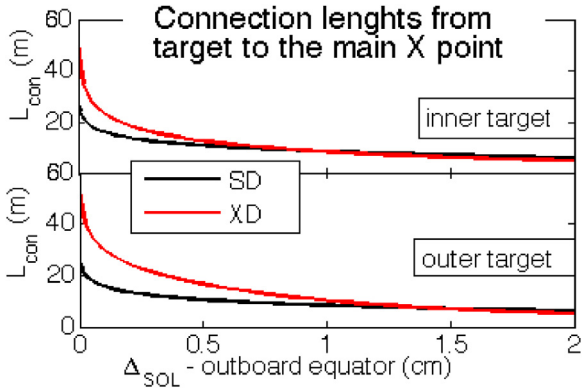

Fig. 4. Connection lengths for SN (black) and XD (red) on both divertor legs versus the outboard equatorial SOL depth. (For interpretation of the references to colour in this figure legend, the reader is referred to the web version of this article.)

Actually other configurations have been developed for DTT, as double null (DN), the SF minus and SF plus together with their variants distinguishing for extension, shape and depth of the B_{pol} null region in between the X points. Here we fix our attention on the XD configuration since it shows as a promising tool for mitigating the target heat loads, still maintaining a high degree of compatibility for divertor design in common with SN. This mitigation has been found in a recent preliminary experiment on the EAST tokamak and has successfully been reproduced by TECXY [25]. Strong XD mitigating properties have also been found in previous modelling studies for the proposed FAST tokamak [29] and for the planned EAST scenarios [25]. These papers also show that not only spreads the load over a larger surface, but could also induce a significant increase of the volume power losses inside the SOL, consequent to the increase of the total connection length L_c of the magnetic field lines. This is in turn caused by their enhanced toroidal twist due to the lower poloidal field mainly in the divertor region, as the larger flux expansion attests. The longer L_c, and hence of the particle dwell time, favour the dissipative inter-particle interactions.

In the present case comparison of the connection lengths between XD and SN is presented in Fig. 4 versus the outer equa-

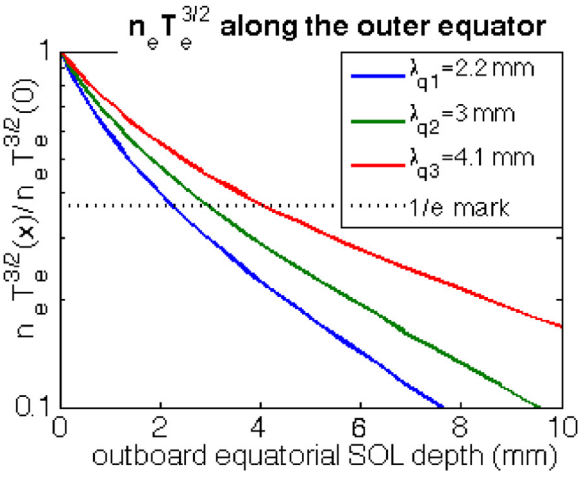

Fig. 5. Radial fall-off of $n_e \times T_e^{3/2}$ on the outer equator for the SN, well attached case for the three couples of cross-field diffusion coefficients given in the text.

torial distance from the separatrix for both the divertor legs. The length is calculated form the target position to the main X point

2.1. Main assumptions for the code inputs

The exploration of the operating parameters has been carried out by performing a density scan on the value at the stagnation point onto the separatrix, $n_{e,s}$. Stagnation is defined as the symmetry point where the fluid velocity is 0 and has opposite directions on either side. The scan is carried out between approximately $0.5 \leq n_{e,s} \leq 1.3 \times 10^{20}$ m^{-3} for each of the three selected couples of values of $(D_\perp, \chi_\perp) = (0.10, 0.25) - (0.15, 0.35) - (0.50, 0.50)$ m^2/s, being $D_\perp$ and $\chi_\perp$ the cross-field diffusion coefficients respectively of particles and heat (both electrons and ions). These three couples give an upstream e-folding decay length $\lambda_{q||,u.s} = 2, 3, 4$ mm for the cross-field profile of the quantity $n_e \times T_e^{3/2}$, shown for the SN reference case in Fig. 5. This quantity indeed best approximates the power flow channel width when the parallel temperature gradient, and conductive heat transport with it, is negligible, as it is usual in the equatorial plane for strongly heated plasmas. This is the same criterion assumed for the recent EUROfusion DEMO assessment [26]. These values of $\lambda_{q||,u.s}$ must be compared with the value $\geq$2.5 mm for the width inside the divertor, mapped at the outer midplane, given by the empirical 0D scaling laws used for dimensioning DTT [11]. Possibility to reach 3 mm is not to be excluded. This value also is consistent with a width resulting from the length of the poloidal ion gyro radius ($\approx$2 mm) + diffusion into the private region, which is neglected in the present TECXY simulations. Clearly, different single values for $D_\perp$ and $\chi_\perp$ can produce the same $\lambda_{q||,u.s}$ and also originate different profiles of n_e and T_e.

The above density scans are fully repeated for the maximum foreseen power crossing the separatrix namely $P_{SOL} = 35$ MW and

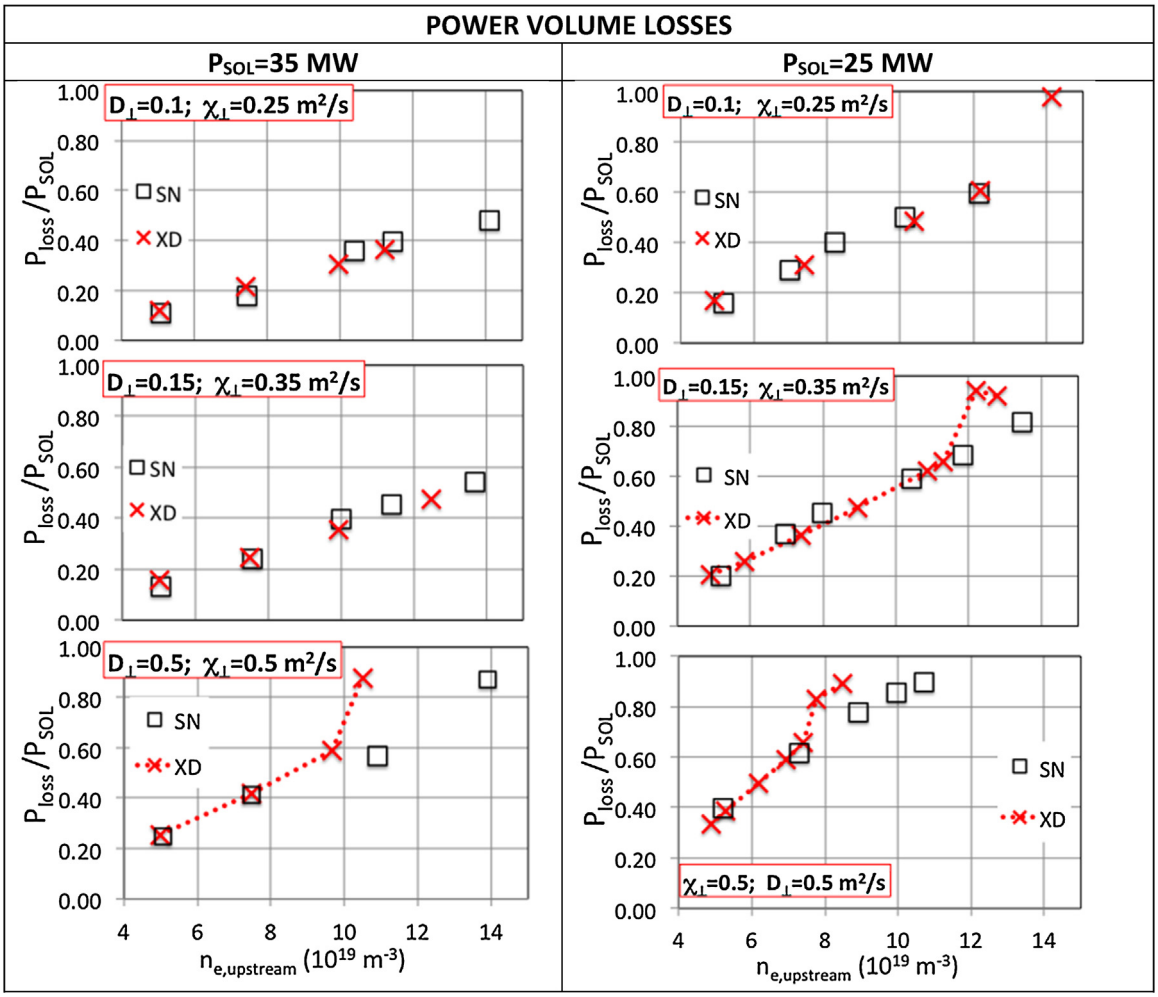

Fig. 6. Ratio of the total volume power losses to the power input into the SOL versus the upstream separatrix density for the three different couples of cross-field transport and for two different power entering the SOL, namely $P_{SOL} = 35$ MW (left column) and $P_{SOL} = 25$ MW (right column).

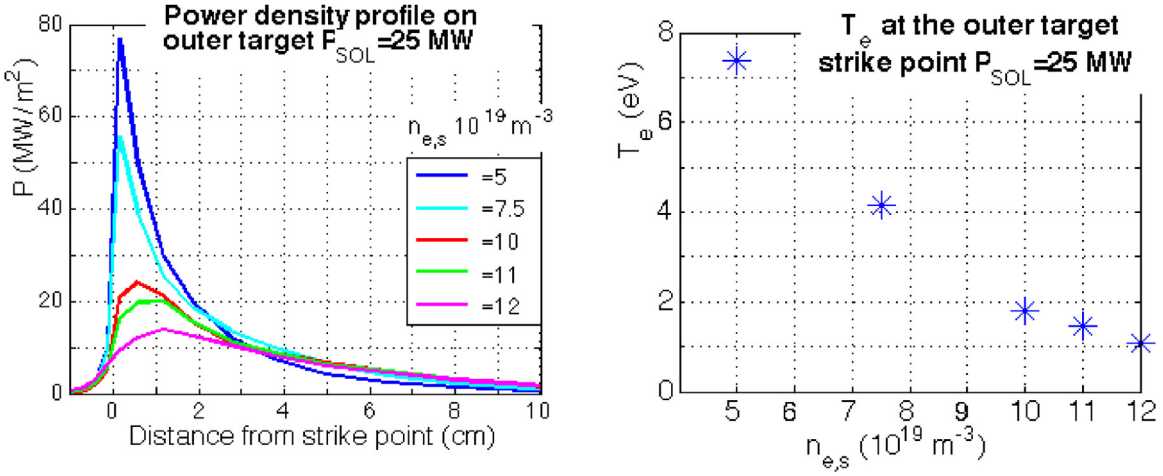

Fig. 7. Simulations from EDGE2D-EIRENE for the DTT standard SN configuration, P_{SOL} = 25 MW, outer target. A) left: Power deposition profiles versus the distance from the strike point; B) right electron temperature at the strike point.

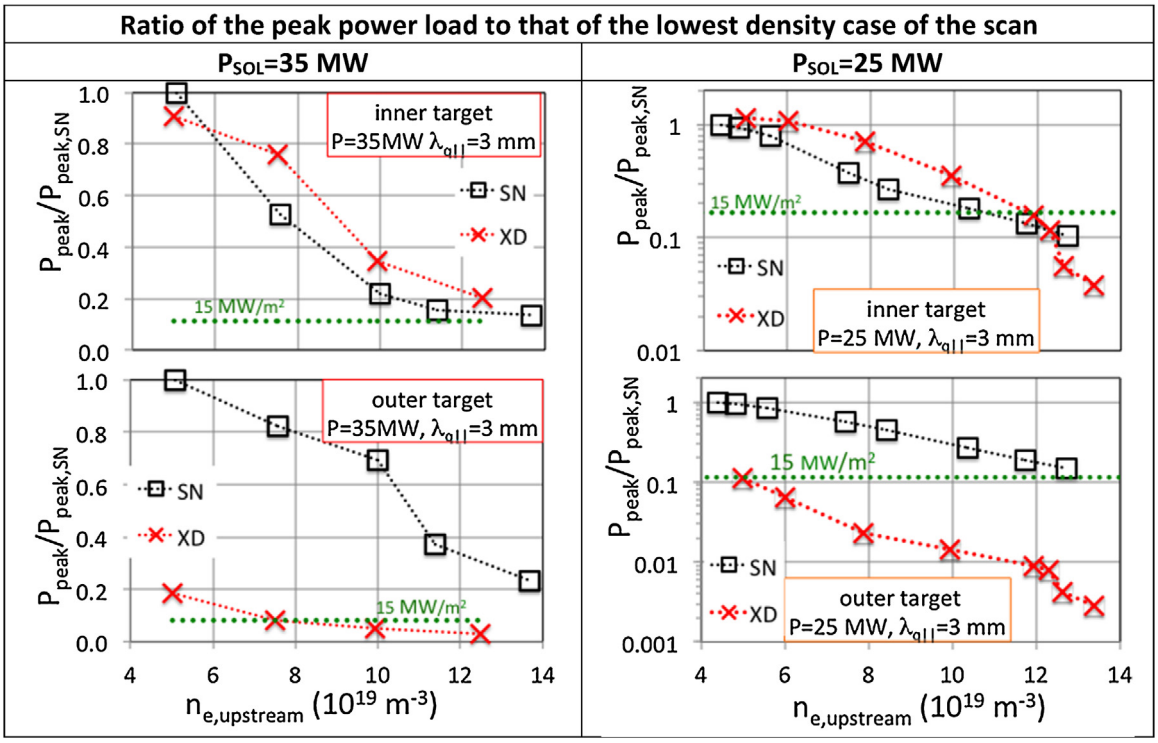

Fig. 8. Mitigation factor for the peak load versus the upstream separatrix density for two different power entering the SOL, namely P_{SOL} = 35 MW (left column) and P_{SOL} = 25 MW (right column). Inner targe on top, outer target on bottom. The given value of 15 MW/m² is simply given by the mitigation factor neded for the lower density peak in case of SN to reach just this value. The transport coefficient considered are $D_\perp$ = 0.1; $\chi_\perp$ = 0.25 m²/s, corresponding to $\lambda_{q||} \approx 3$ mm.

for a bit less value, namely P_{SOL} = 25 MW, giving for the figure of merit P/R the respective values of ≈16 and ≈12 MW/m.

2.2. XD versus SN heat loads for the reference standard scenario

As far as the global quantities are concerned the situation is depicted in Fig. 6. Here we compare the fraction of the total volume losses versus the upstream plasma density at separatrix for the cases with P_{SOL} = 35 and 25 MW, respectively on the left and right column. The three frames on each column refer to the three mentioned couples of cross-field diffusion coefficients, sorted from the top on increasing values of $\lambda_{q||,u.s}$.

Comparing the left versus the right column, it is evident how larger power fraction are lost for the lower power case, as a consequence of the lower temperatures, on average, that enhance all the volume losses processes, mostly charge exchange and D line radiation. The increase of the cross section for these processes has also the positive feedback to increase the number of neutrals, i.e. of the centres for the dissipative processes.

where the deposition profiles normalized to the peak value are plotted versus the outer equator SOL depth, in order get rid of flux expansion effect. A well-attached case with the same volume power loss is considered. The XD channel width is much wider than SN in term of poloidal flux coordinate for the OT, whereas it is negligibly different for the IT. The corresponding density and temperature profiles are shown in Fig. 10

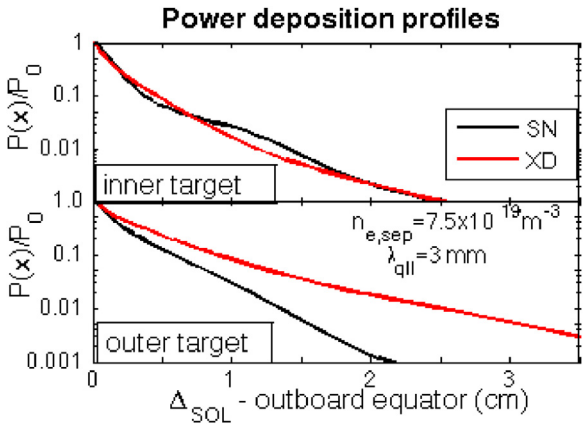

Fig. 9. Normalized power deposition profiles on the inner and outer target, respectively top and bottom frame, mapped versus the outboard equatorial distance.

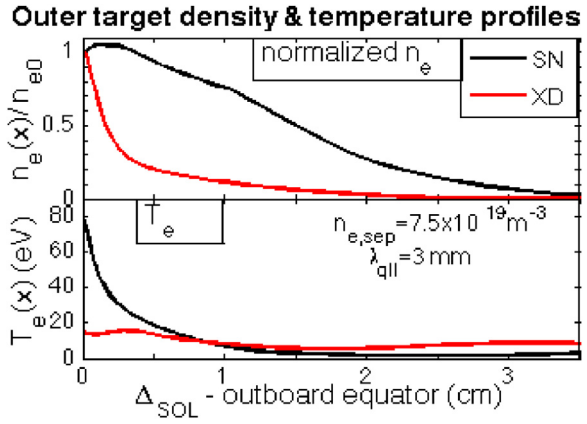

Fig. 10. Profiles on the outer target of density, normalized to the peak (top) and electron temperature (bottom) for the same case considered in the previous figure.

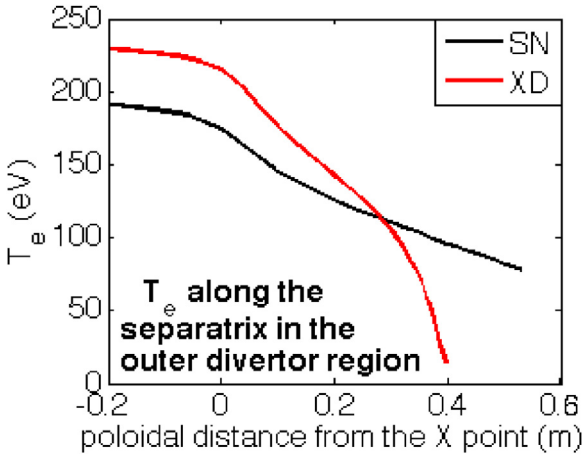

Fig. 11. Variation of the electron temperature along the separatrix from the main X point to target for SN and XD configurations. The parameters of the simulations are the same of the previous figures. – P_{SOL} = 35 MW.

Running along one column it appears that the equivalence between the two configurations can be broken, with a sudden increase of the power loss for XD, mainly linked with the longer connection length (L_{con}) [29,30], for sufficiently long $\lambda_{q||,u.s}$. This is a strong indication of start of, or at least of conditions very close to, detachment. Indeed not only detachment implies a drop of the target load, but is also accompanied by a strong reduction of the temperature, as described in a more detailed study of the main advanced configurations realizable in DTT [30]. This feature is confirmed by simulations with more complete code EDGE2D-EIRENE for the SN configuration. They not only have shown that the power load peak values agree quite satisfactorily with TECXY but also show the contemporary appearance at the strike point of a T_e drop below 2–3 eV and sudden fall of the power load as features of the detachment onset, is observed at $n_{e,s} \approx 1.1 \times 10^{20}$ m^{-3}, see Fig. 7. This density value is the same as the XD detachment in TECXY (middle frame of the right column of Fig. 6), which however does not predict a sudden detachment for SN. We interpret these facts as an indication the present TECXY estimates are quite conservative, i.e. an even earlier XD detachment is not excluded.

The detachment features occur earlier in density for the lower P_{SOL} case, as expected. For the reference case $\lambda_{q||,u.s}$ = 3 mm we note that the density "threshold value" is slightly above the expected range of variability. However for a non-conventional XD configuration it is rather likely to attain higher separatrix density than SN for a given average core density, because of the longer L_{con}. This is expected on the basis of both the experimental results on the tokamak FTU [31] and the present simulations, which require or XD a lower particle flux entering the SOL for the same $n_{e,s}$.

The mitigations that are obtained in the different situations are plotted in Fig. 8, as the ratio of the peak value to the lowest density SN case. In the left (right) column there is the case with P_{SOL} = 35 (25) MW, in the upper (lower) frame there is inner (outer) target. The mitigation required for a sustainable load of 15 MW/m^2 is given for reference as a horizontal green line. We recall, however, that this are loads on target set perpendicular to B_{pol} and therefore are an upper limit to the load, whose actual value is subjected to the real target positioning. The mitigation with XD is always much larger on the outer target than on the inner one, where even an increase with respect to SN can be found. This is the result of the less expansion on IT and of the fact the longer connection lengths shift the stagnation point towards the OT and then the total power conveyed to the IT increases. Neglecting the effect of the plate tilting, for P_{SOL} = 35 MW the load is hardly sustainable on the inner target for both configurations, whereas for OT it is again very hard for SN but becomes sustainable at moderate values of $n_{e,sep}$ for XD. For P_{SOL} = 25 MW the sustainability is much easier except for OT, SN case. For this value of P_{SOL} also the transition to detached case for XD is marked by a sudden drop of the load that occurs on both targets almost simultaneously.

The reason why there is a large drop in the OT for XD case are not only due to the flux expansion, but in large part also to the different width of the power flowing channel in terms of flux coordinates that is induced by the increase of the connection lengths. This is evidenced in Fig. 9 for the OT only. Density is normalized to its peak value. Clearly the spreading of the power is due to the temperature spreading, due to the different magnetic topology. Density adjusts its value in order to keep the pressure profile as requested by the equilibrium equations along the flux line. The main reason for this large T_e radial broadening is to be attributed to a significant variation occurring in the conductive parallel transport. The possible decrease of the target temperature and also of the average value along the flux tube can drop significantly the parallel conductivity. In addition, the longer length can also decrease the parallel T_e gradient along the real flux tube that further slows down the energy transport. Consequently the flow channel width must expand to ensure the same total transport rate. A critical analysis of this issue is carried out in the paper describing all the most relevant advanced divertor configurations that DTT can realize [30]. In support of this view Fig. 11 compares the behaviour of the temperature at the separatrix for SN and XD as a function of the poloidal distance from the main X point. The temperature drop to the OT is quite evident XD. We also remind that the actual flux tube lengths are quite dif-

ferent, despite the same poloidal length, as can be seen from Fig. 4. The modified sharing of the power between the inner and outer legs should also affect this change. A power increase tends to hinder this change, as it apparently happens for the inner target, a decrease instead tends to favour the change.

3. Conclusions

The possible scenarios at full power of the proposed device have been analyzed for the aspect of safely handling the power to be exhausted on the divertor targets. In this conceptual design phase the computational tools have been chosen mainly on the basis of their simplicity and rapidity. This allows outlining in a reasonable time the general features of the problem and giving indications to a subsequent more rigorous analysis. The code COREDIV was used for a preliminary self-consistent description of the coupled edge-core system. Subsequently, a more punctual analysis has been carried out on the SOL. Only the steady state, where ELMs are neglected, is considered and focus is cast on the highest heat load cases, when no impurity is injected to sustain the radiative dissipation of the injected power. In this case the results, indicate that the peak loads are not sustainable in SN configuration at low density, are borderline for the reference case – crucial then becomes the plates tilting – and reach a manageable value at high density.

The difference with COREDIV that predicts for all scenarios quite similar loads is essentially in the fact that TECXY takes into account the actual magnetic topology and then better estimates the volume losses inside the SOL. Therefore, the possible scenarios at full power and a bit reduced one of the proposed DTT have been analysed by TECXY with the main aim to elucidate differences in the power deposition issues between the standard divertor configuration and the advanced one, which can be classified either as an expanded divertor, or a quasi-snow flake. The still lacking final design of the divertor does not make very meaningful using complex codes that would need the details of the divertor layout, namely shape, baffles, pump and so on, in order to be actually reliable. Furthermore, these tools are quite unpractical for exploring the possible working parameter space, due to their quite long running times. We have identified the 2D code TECXY as a good compromise for this phase of the project and the most appropriate tool for our purposes. As pointed out before, the simplified neutral treatment of the neutral dynamics does not allow to describe properly a situation where the role of the neutrals is dominant, as in detached conditions, but still allows to identify the conditions where such detachment is approached, as supported by the EDGE2D-EIRENE simulations. Further, the lack of a final design has led us to consider a conventional, very simplified, divertor geometry with the targets perpendicular to the poloidal field line. Therefore the absolute numbers for the loads are not fully meaningful, whereas their variation with the main plasma parameters can be reliably traced. Furthermore we limited at this stage our analysis to the impurity non-seeded case, since this situation is the most interesting one for the figure of merit P/R that can even exceed the ITER value.

The main outcome of this study is that in term of global parameters little difference exists between the two configurations for low working densities. The reason is identified in the fact that the topology modifications occur in region where the dissipative processes, radiation inelastic collisions etc., are rather negligible to be enhanced at significant level.

The situation shows different at higher density where the XD seems indeed to favour detached operations and strongly radiating regimes. This trend is reinforced by lowering the power entering the SOL and by faster cross-field diffusion. These very important regimes seem to be reachable by the advanced configurations of DTT, for some appropriate choice of the working parameters. Indeed, it is to stress that comparing the two configurations for the same value of separatrix density may be not fully consistent, since for a fixed volume average density, we expect higher edge density for XD, which goes in the right direction towards detachment. While the detailed mechanism for this fact to occur is still matter of investigation, it appears that a crucial role is played by the enhanced cross filed diffusion of the power channel induced by increasing the connection lengths. The temperature suffers a large radial broadening that can drop its value at target to values high enough to enhance significantly all the volume losses.

In the regimes far from detachment the flux expansion plus the T_e spreading just described are quite promising for a safe operation of the targets below the technological limits for the power handling for XD, especially at moderate/high density. Conversely it seems problematic the operation with SN without some independent mechanism to improve radiation, e.g. impurity seeding. However a final assessment on this point clearly claims for a definition of the plate geometry.

We can then expect that further optimization of the position of the secondary nulls on both legs could significantly improve the divertor characteristics from the exhaust point of view, as even already seen on the EAST experiment [25].

Acknowledgements

This work has been carried out within the framework of the EUROfusion Consortium and has received funding from the Euratom research and training programme under grant agreement No 633053. The views and opinions expressed herein do not necessarily reflect those of the European Commission. This scientific work was financed within the Polish framework of the scientific financial resources in 2016 allocated for realization of the international co-financed project.

References

[1] G. Federici, et al., Fusion Eng. Des. 89 (2014) 882.
[2] R. Wenninger, et al., Nucl. Fusion 57 (2017) 016011.
[3] F. Crisanti, et al., The DTT Device: Rationale for the choice of the Parameters, submitted to FED.
[4] R. Stankiewicz, R. Zagórski, J. Nucl. Mater. 313–316 (2003) 899.
[5] R. Zagórski, H. Gerhauser, Phys. Scr. 70 (Part (2/3)) (2004) 173.
[6] S. Wiesen, EDGE2D/EIRENE code interface report, June, 2006, www.eirene.de.
[7] M. Fichtmüller, et al., Contrib. Plasma Phys. 38 (1–2) (1998) 284–289.
[8] J.F. Artaud, et al., 32nd Conf. On Plasma Pohysics and Controlled Fusion and Plasma Physics, ECA V. 29C, P1.035, 2005.
[9] J.G. Cordey, et al., Plasma Phys. Control. Fusion 39 (1997) B115–B127.
[10] S.I. Braginskij, in: M.A. Leontocvich (Ed.), Review of Plasma Physics, Vol. 1, Consultants Bureau, New York, 1965, p. 205.
[11] T. Eich, et al., Phys. Rev. Lett. 107 (2011) 215001.
[12] R. Zagórski, et al., Contrib. Plasma Phys. 48 (2016) 179–184.
[13] R. Zagórski, et al., J. Nucl. Mater. 390–391 (2016) 404.
[14] G. Telesca, et al., J. Nucl. Mater. 438 (July) (2013) S567.
[15] R. Zagórski, et al., Contrib. Plasma Phys. 52 (2012) 379.
[16] V. Pericoli Ridolfini, et al., Fusion Eng. Des. 88 (2013) 1677–1681.
[17] D. Reiter, et al., Fusion Sci Technol. 47 (2005) 172.
[18] V. Rozhansky, et al., Nucl. Fusion 49 (2009) 025007.
[19] H. Bufferand, et al., J. Nucl. Mater. 438 (2013) S445–S448.
[20] T. Lunt, et al. Optimisation of the snowflake divertor by means of EMC3-Eirene simulations', submitted to Plasma Phys. Contr. Fusion.
[21] R. Zagórski, J.P. Gunn, I. Nanobashvili, Plasma Phys. Control. Fusion 49 (2007) S97–S108, online at: stacks.iop.org/PPCF/49/S97.
[22] V. Pericoli-Ridolfini, M.L. Apicella, G. Mazzitelli, O. Tudisco, R. Zagórski, the FTU team, Plasma Phys. Control. Fusion 49 (2007) S123–S135, online at: stacks.iop.org/PPCF/49/S123.
[23] H. Gerhauser, R. Zagórski, H.A. Claaßen, G. Mank, T. Loarer, J. Gunn, C. Boucher, Plasma Phys. Control. Fusion 42 (2002) 805, online at: stacks.iop.org/NF/42/805.
[24] H. Gerhauser, R. Zagórski, S. Jachmich, M. VanSchoor, J. Nucl. Mater. 313–316 (2003) 893–898 (online at:) www.sciencedirect.com/science/article/pii/S0022311502014721.
[25] G. Calabrò, B.J. Xiao, S.L. Chen, Y.M. Duan, Y. Guo, J.G. Li, L. Liu, Z.P. Luo, L. Wang, J. Xu, et al., Nucl. Fusion 55 (8) (2015) 083005, http://dx.doi.org/10.1088/0029-5515/55/8/083005, on line at: stacks.iop.org/NF/55/083005.

[26] H. Reimerdes, et al., Assessment of the DEMO compatibility of alternative plasma exhaust solutions, in: EUROfusion report for WP-DTT1, 2016, December.
[27] G. Rubino, R. Ambrosino, G. Calabrò, V. Pericoli Ridolfini, B. Viola, Comparative analysis of the SOL plasma in DEMO using EDGE2D/EIRENE and TECXY codes, in: 22nd Intern. Conf. on Plasma Surface Interactions in Controlled Fusion Devices, Rome, Italy, 30 May–3 June 2016, 2016, submitted to Nuclear Materials and Energy.
[28] F. Subba, L. Aho-Mantila, R. Ambrosino, D.P. Coster, V. Pericoli-Ridolfini, A. Uccello, R. Zanino, Efficiency of non-standard divertor configurations in DEMO, in: 22nd Intern. Conf. on Plasma Surface Interactions in Controlled Fusion Devices, Rome, Italy, 30 May–3 June 2016, 2016, submitted to Nuclear Materials and Energy.
[29] V. Pericoli Ridolfini, et al., J. Nucl. Mater. 438 (2013) S414–S417, http://dx.doi.org/10.1016/j.jnucmat.2013.01.083.
[30] V. Pericoli Ridolfini et al. Effect of the magnetic topology of a tokamak divertor on the power exhaust properties, submitted to Physics of Plasmas.
[31] M. Leigheb, V. Pericoli Ridolfini, R. Zagórski, J. Nucl. Mater. 241–243 (2017) 914–918, http://dx.doi.org/10.1016/S0022-3115(97)80165-1.